J Mater Sci (2008) 43:5123–5130
DOI 10.1007/s10853-008-2738-3

Synthesis of magnetite nanoparticles by thermal decomposition of ferrous oxalate dihydrate

Andre Angermann · Jörg Töpfer

Received: 10 January 2008 / Accepted: 16 May 2008 / Published online: 7 June 2008
© Springer Science+Business Media, LLC 2008

Abstract Two different polymorphs of ferrous oxalate dihydrate were synthesized by precipitation of ferrous ions with oxalic acid: α-$Fe(C_2O_4) \cdot 2H_2O$ with a monoclinic unit cell is obtained after precipitation and ageing at 90 °C, whereas the orthorhombic β-type is formed after precipitation at room temperature. The morphology of the oxalate crystals can be tailored from prismatic crystals of the α-polymorph over star-like aggregates of α/β-mixtures to non-agglomerated crystallites of β-oxalate. Thermal decomposition in air gives hematite at $T \geq 250$ °C; if the thermolysis reaction is performed at low oxygen partial pressures (e.g., $T = 500$ °C and $p_{O2} = 10^{-25}$ atm) magnetite is obtained. The synthesized magnetite is stoichiometric as signaled by lattice parameters of $a_0 = 8.39$ Å. The thermal decomposition of ferrous oxalate is monitored by thermal analysis, XRD, and IR-spectroscopy. The morphology of the oxalate crystals is preserved during thermal decomposition; the oxalates are transformed into spinel particle aggregates of similar size and shape. The crystallite size of the magnetite particles increases with temperature and is 40 or 55 nm, if synthesized from β-oxalate at 500 °C or 700 °C, respectively. The saturation magnetization of the magnetite particles decreases with decreasing particle size. Since the particles are larger than the critical diameter for superparamagnetic behavior they display hysteresis behavior at room temperature.

A. Angermann · J. Töpfer (✉)
Department of SciTec, University of Applied Sciences, Carl-Zeiss-Promenade 2, Jena 07745, Germany
e-mail: joerg.toepfer@fh-jena.de

Introduction

Ferrous oxalate dihydrate $Fe(C_2O_4) \cdot 2H_2O$ has been shown to be identical with the mineral Humboldtine many years ago [1]. The crystal structure was investigated by Mazzi et al. [2] and Carić [3]. Two polymorphs were described by Deyrieux and Peneloux [4]: α-ferrous oxalate (Humboltine) has a monoclinic unit cell, space group C2/c (no. 15), and $a_0 = 12.05$ Å, $b_0 = 5.57$ Å, $c_0 = 9.76$ Å, and $\beta = 124°18'$ with $z = 4$. The β-polymorph has an orthorhombic cell, space group Cccm (no. 66), with $a_0 = 12.26$ Å, $b_0 = 5.57$ Å, and $c_0 = 15.48$ Å and $z = 8$. The α- and β-oxalates were synthesized by precipitation from ferrous salt solutions with oxalic acid either with excess or stoichiometric oxalate/iron ratios, respectively [4]. The thermal decomposition of ferrous oxalate has been studied by many authors (e.g. [5–11]). The results of older papers were rather controversial regarding the decomposition products in various atmospheres. As an example, Rao et al. [5] observed α- or γ-Fe_2O_3 after oxalate decomposition in air depending on the degree of moisture. Today, it is generally accepted that the decomposition product in air is hematite, α-Fe_2O_3, (e.g. [6, 7, 10, 11]). The situation is more complex if decomposition is performed in an atmosphere of inert or reducing gases or in closed containers, where gaseous decomposition products might form quite reducing conditions. Recently, Frost and Weier demonstrated that decomposition under reducing conditions gives magnetite, Fe_3O_4, or iron depending on the partial pressure of oxygen [7]. Decomposition in a gas atmosphere dominated by the own conversion gases was shown to proceed via magnetite and cementite to wüstite and metallic iron [9]. Rod-shaped ferrous oxalate was shown to topotactically transform into maghemite at 400 °C in nitrogen or magnetite in a sealed tube at 400 °C [11].

Magnetite (Fe_3O_4) crystallizes in the spinel structure with ferrous and ferric ions on the octahedral sites of the spinel lattice, space group Fd3m, and a lattice constant of about 8.39 Å [12]. Magnetite particles have gained a lot of attention as candidate materials for biomedical heating applications. It appears that the optimum particle size range is 20–50 nm and it was shown that bacterial magnetosomes with size of 30 nm have large specific loss powers [13]. Commonly, magnetite nanoparticles are prepared by precipitation methods; e.g., an oxydative alcaline hydrolysis reaction of ferrous ions [14, 15]. The precipitation with a base from a solution containing ferrous and ferric ions has often been used to prepare magnetite particles with about 10 nm in size [16–18]. Recently, Mürbe et al. [19] have reported on the preparation of magnetite particles in the size range 20–100 nm by adapting the precipitation conditions. The specific loss powers of these chemically prepared iron oxide nanoparticles have already been reported [20]; they are smaller than those form magnetosomes. Very recently, the synthesis of ellipsoidal hematite and magnetite particles from micro-sized ferrous carbonate particles by topotactical decomposition with preservation of the particle shape was described [21].

In this communication, we report on the synthesis and morphology of ferrous oxalate dihydrate particles. The morphology of the oxalate particles depends on the precipitation conditions. The thermal decomposition in reduced oxygen partial pressure leads to magnetite powders. The shape of the oxalate crystals is transferred into the magnetite particles during the decomposition. The obtained magnetite particles with crystallite sizes in the range of 35–55 nm show hysteresis behavior at room temperature.

Experimental

Sample preparation

Ferrous oxalate dihydrate crystals were prepared by precipitation reactions. Iron powder as starting material was dissolved in an acetic acid solution under argon and subsequently combined with an oxalic acid solution in a stoichiometric ratio. The temperature of precipitation and the duration of aging in argon atmosphere were varied: 1 h at 20 °C, 30 °C, 60 °C, 90 °C, and 7 h at 90 °C. Finally, the oxalates were washed and filtered with distilled water and isopropanol before drying at room temperature in air. Thermal decomposition was performed either in air in a drying chamber or under reduced partial pressure of oxygen (10 K/min heating rate) in a thermobalance. The gas atmosphere was established by $N_2/CO/CO_2$-mixures using mass flow controllers and the oxygen partial pressure was monitored with zirconia cells at the entrance and exit of the TG apparatus.

Characterization

The oxalate and oxide particles were investigated by scanning electron microscopy (SEM; DSM 940A, Zeiss, Jena, Germany) and transmission electron microscopy (TEM; Hitachi H8100). Powder X-ray diffraction measurements (XRD) were performed with a Siemens D5000 and Cu K_α radiation (step time 8 s; step size 0.02°; 10–130° 2θ). Lattice parameters were refined using the TOPAS R software package (Bruker AXS, Karlsruhe, Germany). The crystallite size was estimated from XRD line broadening using the Scherrer equation, $d_{xrd} = K\lambda/[(B\text{-}b)\cos\theta]$, with the wave length λ, the peak width B, the instrumental broadening b ($b = 0.08°$ for standard LaB_6), the Bragg angle θ, and the shape factor $K \approx 0.89$. Thermal analysis (TG, DTA) was carried out with a SETARAM TGA92 system, the samples were heated in open Pt containers (TG + DTA sample holder: diameter 3 mm, height 6 mm) in air or CO/CO_2 to 500 °C with a rate of 2 K/min (sample mass about 20 mg). IR spectra were recorded from 4,000 to 400 cm^{-1} using a Mattson FTIR spectrometer (Genesis II); 3 mg of the powdered samples were diluted with 97 mg KBr.

Magnetic properties were measured with a Quantum Design MPMS SQUID magnetometer. Hysteresis loops were measured at 5 and 298 K. The magnetization at the maximum field of 50 kOe was taken as saturation magnetization M_s.

Results and discussion

The synthesis of the ferrous oxalate dihydrates by precipitation gives yellow powders irrespective of the precipitation temperature and aging time. X-ray diffraction studies show that orthorhombic β-iron-(II)-oxalate dihydrate is observed after precipitation at 20, 30, 60, and 90 °C. The XRD powder pattern of the sample prepared at 20 °C is shown in Fig. 1. All diffraction peaks could be indexed in the orthorhombic structure (space group Cccm) as proposed by Deverieux et al. [4]; no additional reflections were observed. The calculated lattice parameters are $a_0 = 12.223(4)$ Å, $b_0 = 5.556(2)$ Å, and $c_0 = 15.438(5)$ Å and agree well with those in ref. [4]. Precipitation and aging for 7 h at 90 °C leads to the monoclinic α-polymorph (Fig. 1) with the refined unit cell dimensions $a_0 = 11.998(2)$ Å, $b_0 = 5.546(1)$ Å, $c_0 = 9.900(2)$ Å, and $\beta = 128°59(3)'$. The α-ferrous oxalate seems to require a formation temperature of 90 °C for some time for complete transformation; several experiments at

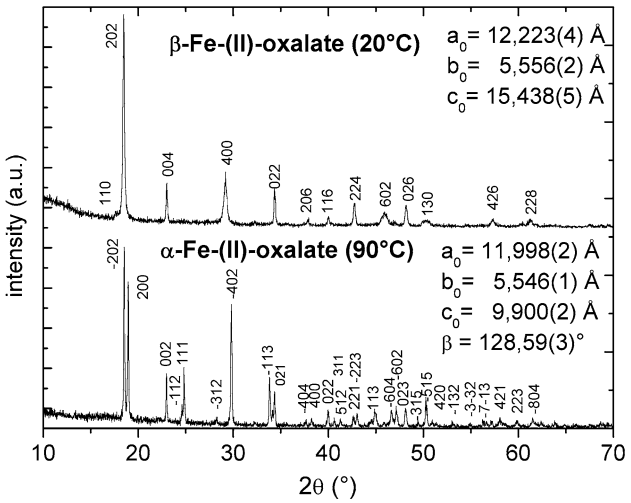

Fig. 1 XRD pattern of ferrous oxalate dihydrate: β-oxalate obtained at 20 °C (upper part) and α-oxalate obtained at 90 °C (lower panel)

90 °C with aging periods between 1 and 7 h resulted in mixtures of α- and β-oxalates.

The morphologies of the ferrous oxalate crystals vary with the synthesis conditions. The β-oxalate precipitated at room temperature consists of loosely agglomerated particles with a primary particle size in the order of 200–600 nm as demonstrated by SEM micrographs in Fig. 2a. Precipitation at increased temperature leads to the formation of larger agglomerates; typical features are bar-shaped crystals several microns in length that form star-like aggregates (Fig. 2b). In contrast, the α-ferrous oxalate formed at 90 °C has prism-shaped crystals of 1–2 μm size (Fig. 2c) resembling a typical habitus of crystals with a monoclinic unit cell.

IR spectra of the two polymorphs (Fig. 3) display the typical absorption bands of metal oxalate hydrates; i.e., a strong band at 3,500 cm^{-1} for hydrated water and a band at 1,630 cm^{-1} that is due to antisymmetric ν(C=O) stretching vibration modes. Bands at 1,300 and 800 cm^{-1} are characteristic of O–C–O stretching and bending modes, respectively [7, 22].

The thermal decomposition of ferrous oxalate dihydrate in air as monitored by TG and DTA is shown in Fig. 4a (α- and β-ferrous oxalate hydrates show identical TG and DTA curves). A mass loss sets in at 150 °C and is almost completed at 300 °C. The total mass loss of 55.5% at

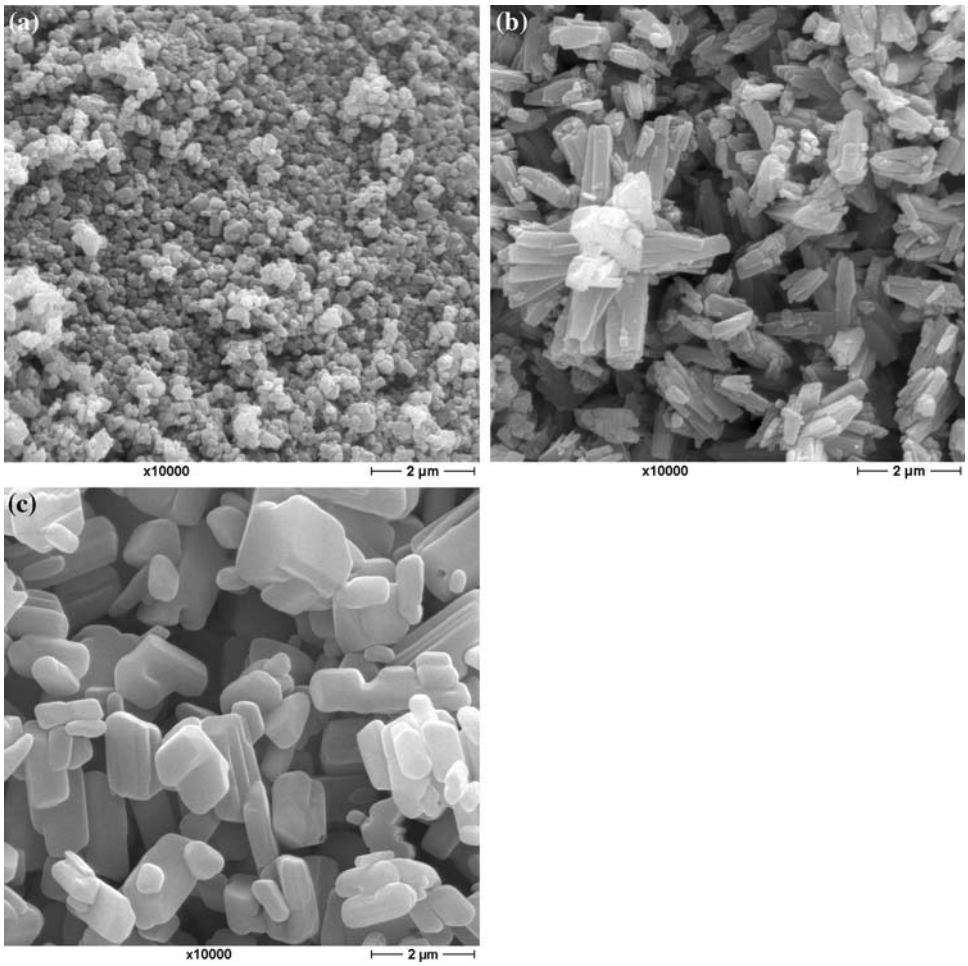

Fig. 2 SEM micrographs of ferrous oxalate dihydrates prepared at 20 °C (**a**), 60 °C (**b**) and 7 h at 90 °C (**c**)

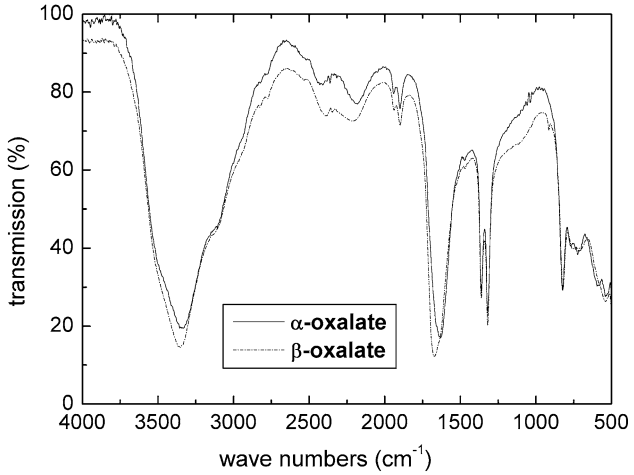

Fig. 3 Infrared spectra of α- and *β*-ferrous oxalate dihydrates (prepared 7 h at 90 °C for the α- and 1 h at 20 °C for the *β*-oxalate, respectively)

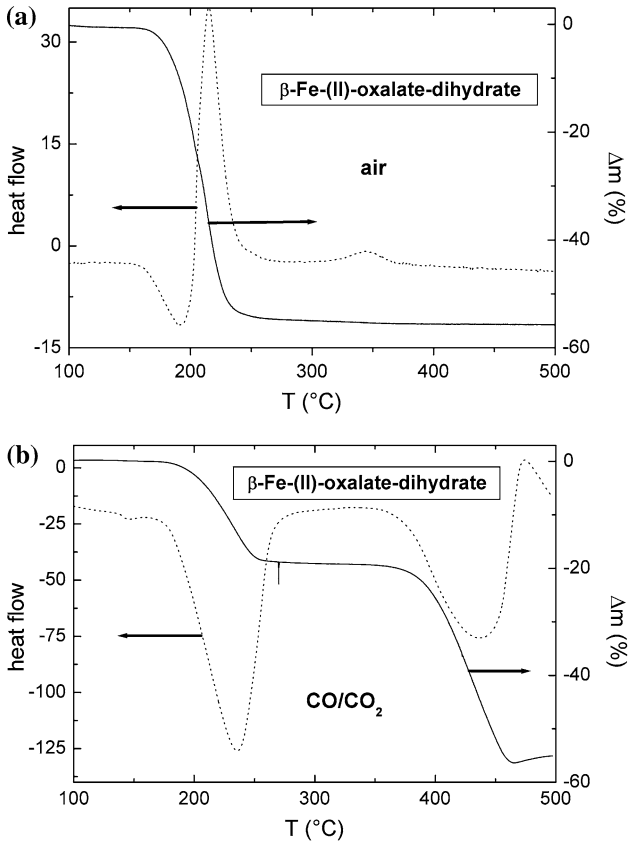

Fig. 4 Thermal analysis (TG and DTA) of *β*-ferrous oxalate dihydrate in air (**a**) and CO/CO_2 gas mixture (**b**); heating rate 2 K/min

400 °C agrees well with a calculated loss of 55.6% for the decomposition reaction:

$$FeC_2O_4 \cdot 2H_2O + {}^1\!/_4O_2 \rightarrow {}^1\!/_2Fe_2O_3 + CO + CO_2 + 2H_2O \quad (1)$$

The DTA curve exhibits an endothermic signal peaking at 180 °C signaling the dehydration step. A sharp exothermic peak at 215 °C corresponds to the decomposition reaction. This is in good agreement with earlier studies [6, 8]. A small exothermic signal at 340 °C might indicate crystallization of hematite. Such a transition from amorphous to crystalline hematite after decomposition of ferrous oxalate in air was observed by Mössbauer and XRD experiments [10].

If the decomposition is performed in a 1% CO/99% CO_2 gas mixture (Fig. 4b), the dehydration reaction sets in at 170 °C and the corresponding endothermic DTA signal is centered at 240 °C. At 300 °C a mass loss of 19.9% corresponding to complete dehydration is reached. Oxalate decomposition starts at 350 °C and is finished at 470 °C at a total mass loss of 57.0% which agrees well with the theoretical 57.1% for magnetite formation as a result of oxalate decomposition:

$$FeC_2O_4 \cdot 2H_2O + 1/6O_2 \rightarrow 1/3Fe_3O_4 + CO + CO_2 + 2H_2O \quad (2)$$

A broad endothermic peak with the maximum at 430 °C accompanies this reaction. On further heating, a distinct weight increase of about 2% up to the final temperature of 500 °C accompanied by an exothermic peak appears. This is likely to be due to partial oxidation to maghemite as a result of the formation of a local gas atmosphere in the TG/DTA crucible that is slightly less reducing (CO/CO_2-ratio smaller than 1/99) and hence leads to some oxidation.

To study the properties of the iron oxide formed as a result of oxalate decomposition, 1 g of *β*-ferrous oxalate dihydrate was decomposed at 450 °C for 4 h in air in a flat Pt container (diameter 100 mm, material layer thickness about 2 mm). XRD analysis of the decomposition product confirms the formation of hematite (Fig. 5) as expected from the TG study.

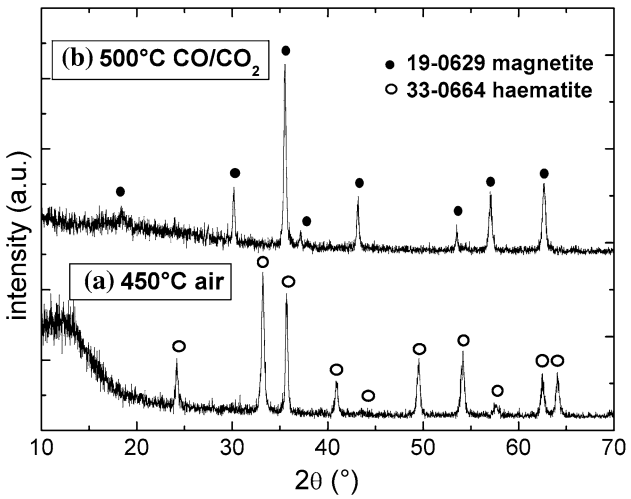

Fig. 5 XRD pattern of *β*-ferrous oxalate dihydrate decomposed at 450 °C in air (a) and at 500 °C in CO/CO_2 (b)

To obtain magnetite Fe_3O_4 as a result of ferrous oxalate decomposition, the oxygen partial pressure has to be reduced according to the phase diagram of the system Fe–O [23]. Since we are interested in the preparation of nanosize magnetite particles, decomposition temperatures of 500 and 700 °C were selected. The corresponding oxygen partial pressures of 10^{-25} and 10^{-18} atm [23], respectively, were generated by CO/CO_2 mixtures. Samples of about 200 mg of β- and α-ferrous oxalate (synthesized at 1 h at 20 °C and 7 h at 90 °C, respectively) were heated on open Pt crucibles (TG sample holder, diameter 10 mm, height 4 mm) in the thermobalance with 10 K/min to 500 or 700 °C in CO/CO_2 atmospheres, respectively, and held there for 4 h. Then the samples were rapidly cooled in the furnace to avoid phase decomposition since the p_{O2} is temperature dependent for a fixed CO/CO_2-ratio. Contrary to the dynamic TG/DTA run (Fig. 4b), in this case the TG signal remained constant at T (470 °C at $\Delta m = 57\%$ indicating that the use of a broader crucible prevented the formation of local oxidizing gas atmospheres; moreover, the 4 h holding time was sufficient to establish a gas atmosphere with the desired p_{O2}. As an example, the XRD-pattern of the iron oxide powder obtained after decomposition of β-Fe-(II)-oxalate at 500 °C in CO/CO_2 is shown in Fig. 5; the formation of single phase magnetite is confirmed. The formation of maghemite can be excluded from the XRD data since due to ordering of cation vacancies it crystallizes either in a primitive cubic or tetragonal unit cell with additional reflections compared to the face-centered cubic cell of the Fd3 m spinel lattice of magnetite [12, 19]. The formation of maghemite with a cubic face-centered spinel structure is limited to small crystallites with $d < 12$ nm where vacancy ordering has not been completed yet [19, 24].

The formation of magnetite is confirmed by the lattice parameters of the synthesized iron oxide spinels (Table 1). The calculated unit cell dimensions of $a_0 \approx 8.39$ Å are typical of stoichiometric bulk magnetite; cubic maghemite has $a_0 \approx 8.34$ Å [12, 19]. Calcination of α- and β-oxalates at 700 °C in CO/CO_2 results in pure magnetites with $a_0 = 8.397$ Å, whereas firing at 500 °C gives powders with slightly reduced values of $a_0 = 8.389$ Å indicating that the phase formation is not perfectly complete yet (see Fig. 4b). On the other hand, magnetite nanoparticles prepared by basic precipitation from Fe^{2+}/Fe^{3+} solutions in argon atmosphere commonly exhibit smaller lattice constants of 8.38 Å $\geq a_0 \geq$ 8.34 Å [19]. It was shown that in such case the observed shrinkage of the unit cell dimensions a_0 with decreasing particle size originates from a partial oxidation of magnetite toward maghemite. In the study reported here, the powders were obtained after firing at 500 or 700 °C in corresponding gas atmospheres (i.e., equilibrium oxygen partial pressures of magnetite); therefore, pure magnetite was obtained as indicated by the values of a_0.

From the XRD peak broadening the crystallite sizes of the magnetite powders were calculated (Table 1). The results reveal that nanosize magnetite powders with crystallite sizes in the range 35–55 nm were prepared. As expected, the size increases with oxalate decomposition temperature.

The constitution of the iron oxides prepared by oxalate decomposition in air or CO/CO_2 was also investigated by IR spectroscopy. As an example, the spectra of the oxides obtained by thermal treatment of β-oxalate are shown in Fig. 6. The spectrum of the sample prepared at 450 °C in air shows several distinct bands that allow unequivocal identification of hematite. Strong bands at 550 and 460 cm^{-1} and weaker bands at 630 and 390 cm^{-1} are in good agreement with IR spectra of α-Fe_2O_3 discussed in the literature [25–27]. The IR-spectrum of magnetite (prepared at 500 °C in CO/CO_2) shows one broad absorption band centered at about 570 cm^{-1} only. A factor group analysis reported in a classic IR work on spinels resulted in four IR active bands; in most cases including magnetite only two of them are observed between 400 and

Table 1 Properties of magnetites obtained by thermal decomposition of α- and β-ferrous oxalates at 500 and 700 °C in CO/CO_2 (lattice parameter a_o; crystallite size d_{xrd}; saturation magnetization M_s and coercivity H_c)

Sample	a_0 (Å)	d_{xrd} (nm)	M_s (emu/g)	H_c 5 K (Oe)	H_c 295 K (Oe)
β-500	8.389(2)	40(4)	78.9	370	125
β-700	8.3969(5)	55(2)	85.4	60	55
α-500	8.389(2)	35(4)	–	–	–
α-700	8.3978(6)	50(4)	–	–	–

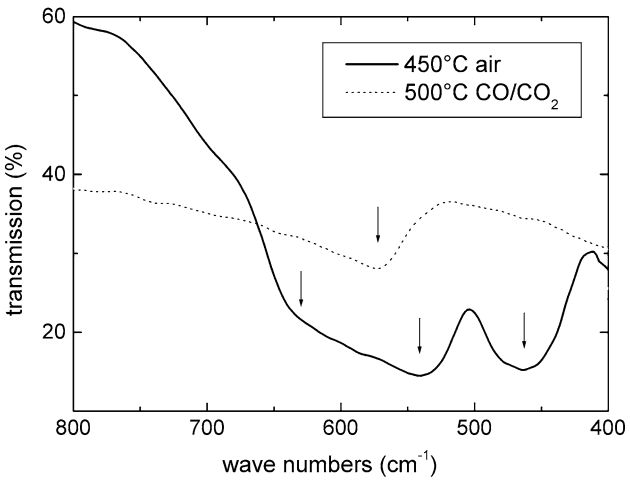

Fig. 6 Infrared spectra between 400 and 800 cm^{-1} of magnetite and hematite obtained by thermal decomposition of β-ferrous oxalate dihydrate at 500 °C in CO/CO_2 atmosphere and at 450 °C in air

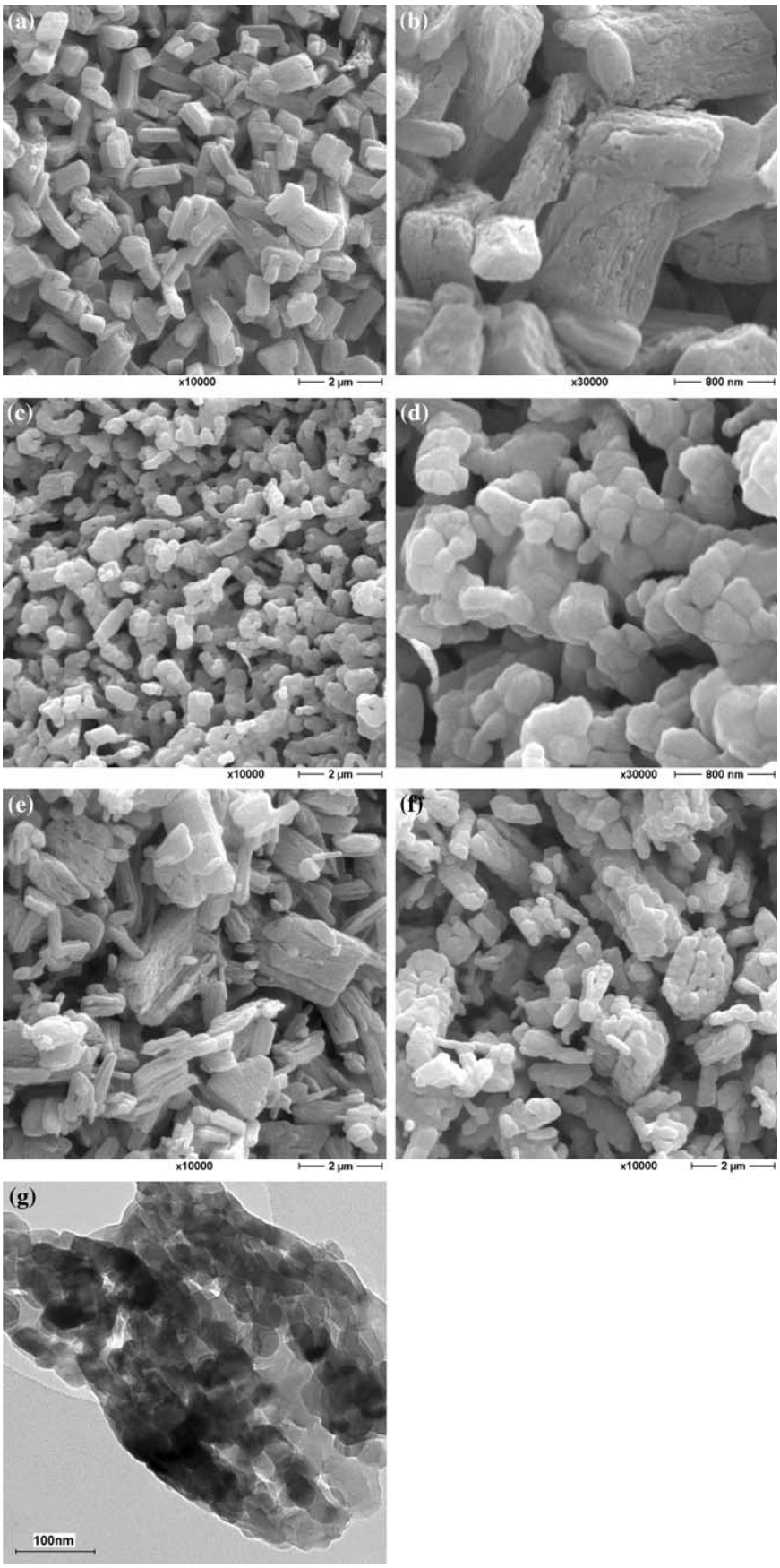

Fig. 7 SEM micrographs of magnetite powders prepared by thermal decomposition of β-ferrous oxalate dihydrate at 500 °C (**a**, **b**) and 700 °C (**c**, **d**) and α-ferrous oxalate dihydrate at 500 °C (**e**) and 700 °C (**f**) and at 500 °C as TEM micrograph (**g**)

800 cm^{-1} [25, 28, 29]. In our spectrum the second band is not observed; obviously this band is located at wavenumbers lower than 400 cm^{-1}.

SEM micrographs of the magnetite powders (Fig. 7) demonstrate that the morphology of the oxalate crystals is preserved during the course of thermal decomposition and has a strong impact on the shape and agglomeration behavior of the magnetite particles. The β-oxalate crystals (precipitated at 20 °C) have transformed into magnetite at 500 °C under grain growth. The obtained magnetite consists of bulky aggregates of 1 μm size (Fig. 7a) that do hardly form bigger agglomerates. The primary particles are visible under higher magnification (Fig. 7b). Magnetite prepared at 700 °C still consists of loose agglomerates; the beginning of sintering has led to some grown aggregates (Fig. 7c) and sintering necks appear between some aggregates (Fig. 7d). In contrast, thermal decomposition transforms the larger prism-shaped α-ferrous-oxalate crystals into a completely different magnetite morphology. Although the primary particles have similar sizes as in the case of magnetites from β-oxalates, this magnetite powder (prepared at 500 °C) contains many hard aggregates of various sizes (Fig. 7e). Magnetite prepared at 700 °C (Fig. 7f) contains many hard aggregates made of crystallites of larger size. If we compare Fig. 7a and e, we can distinguish between two different magnetites (both prepared at 500 °C, but from β- and α-oxalates); both powders consist of aggregates of primary particle of similar sizes, but the aggregates are smaller, more homogeneous in size, and only loosely agglomerated in the case of magnetite from β-ferrous oxalate (Fig. 7a). The crystallites size of 35 nm of magnetite obtained from α-oxalate at 500 °C as determined from X-ray line broadening is nicely confirmed by TEM micrographs (Fig. 7g).

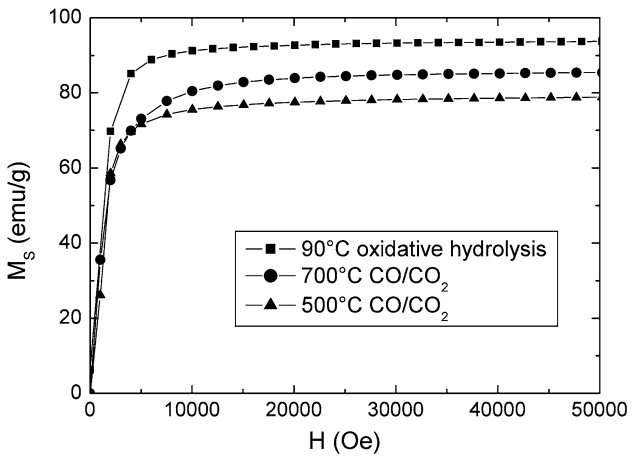

Fig. 8 Magnetization as function of magnetic field for magnetite prepared by thermal decomposition of β-ferrous oxalate dihydrate at 500 and 700 °C; for comparison a magnetite prepared from oxidative hydrolysis with crystal size of 100 nm is shown

The magnetization of the magnetite nanoparticles synthesized from β-oxalate at 500 and 700 °C is shown as a function of magnetic field in Fig. 8. The saturation magnetization (taken as magnetization at the maximum field of 50 kOe) is smaller than the theoretical value for Fe_3O_4 of 96.4 emu/g (assuming an inverse cation distribution and antiparallel alignment of magnetic moments between the A- and B-sites of the spinel lattice). Moreover, M_s becomes smaller with decreasing crystallite size (Table 1) as frequently observed for nanoscale iron oxides (e.g. [19, 30]). For comparison, the $M(H)$ curve of a magnetite prepared by oxidative hydrolysis with particle size of 100 nm is shown: the $M_s = 93$ emu/g is close to that of bulk Fe_3O_4. Since the nanoscale iron oxide samples prepared by oxalate decomposition at 500/700 °C in CO/CO_2 consist of pure and non-oxidized magnetite (as discussed before) the reduced M_s is not likely to be due to oxidized surface layers as being characteristic for samples prepared by precipitation with a base from ferrous/ferric solutions at moderate temperatures in argon [19], but rather due to surface spin disorder effects as suggested by Coey et al. [30].

The hysteresis behavior at 5 and 295 K of magnetite prepared from β-ferrous oxalate dihydrate at 500 °C is shown in Fig. 9. No superparamagnetic behavior was observed. This is in agreement with the fact that the critical size for superparamagnetism in magnetite was reported to be 29 nm [31]. A coercivity of 125 Oe is found at room temperature, which is comparable with a $H_c = 162$ Oe for magnetite nanocrystals as part of ellipsoidal agglomerates prepared by topotactic decomposition of ferrous carbonate [21]. On the other hand, this is significantly larger than the coercivities of about 90 Oe for 40 nm sized magnetite nanoparticles prepared by base precipitation reactions [19]. This coercivity enhancement might be caused by a larger shape anisotropy of the particles formed by topotactic

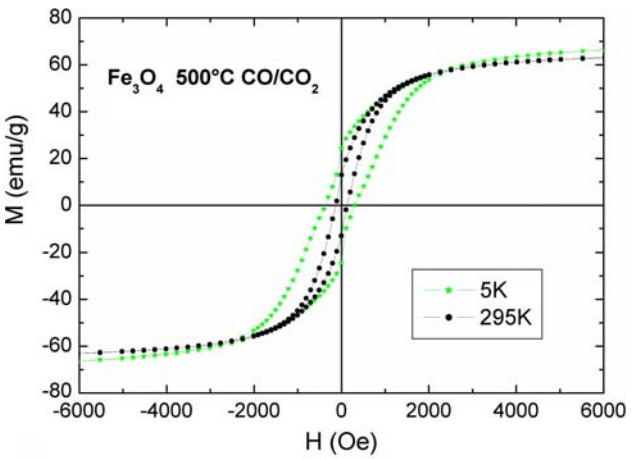

Fig. 9 Magnetic hysteresis loops at 5 and 295 K of magnetite prepared from β-ferrous oxalate dihydrate at 500 °C

carbonate or oxalate decompositions. For the powder obtained at 500 °C from β-oxalate a typical arrangement of individual magnetite crystals into larger aggregates with an aspect ratio of about 5 is observed (Fig. 7b). This type of aggregation behavior is not observed in magnetite prepared at 700 °C (Fig. 7d). Here the aggregates are more rounded and, moreover, the crystallite size is increased to 55 nm; hence the coercivity is drastically reduced to 55 Oe.

Conclusions

Ferrous oxalate dihydrate particles were synthesized by precipitation reactions. Precipitation at 20–90 °C and aging for 1 h results in β-oxalates with orthorhombic structure. If precipitation is performed at 90 °C for 7 h monoclinic α-oxalate is obtained. The oxalate morphology can be tailored from small rounded hardly agglomerated particles to heavily agglomerated powders. Thermal decomposition of the oxalates in air gives hematite as stable reaction product, whereas at sufficiently low oxygen partial pressure magnetite is obtained. The crystallite size of the magnetite obtained at 500 or 700 °C is between 35 and 55 nm. The morphologies of the magnetite particles resemble those of the oxalate crystals; magnetite powders of loosely or heavily aggregated crystallites were observed. The saturation magnetization is smaller compared to bulk magnetite; however, the coercivity is large for particles that form aggregates with an aspect ratio.

Acknowledgements The authors thank Mrs. S. Müller and M. Friedrich (FH Jena) for oxalate preparations and SEM investigations, respectively.

References

1. Manasse E (1910) Rend Acc Naz Lincei 19:138
2. Mazzi F, Garavelli C (1957) Period Mineral 26:269
3. Carić S (1959) Bull Soc franc Min Crist 82:50
4. Deyrieux R, Peneloux A (1969) Bull Soc Chim Fr 8:2675
5. Rao V, Shashimohan AL, Biswas AB (1974) J Mater Sci 9:430–433. doi:10.1007/BF00737843
6. Glenn Rupard R, Gallagher PK (1996) Thermochim Acta 272:11. doi:10.1016/0040-6031(95)02626-6
7. Frost RL, Weier ML (2004) J Therm Anal Calorim 75:277. doi:10.1023/B:JTAN.0000017349.31035.dd
8. Mohamed MA, Galwey AK, Halawy SA (2005) Thermochim Acta 429:57. doi:10.1016/j.tca.2004.08.021
9. Hermanek M, Zboril R, Mashlan M, Machala L, Schneeweiss O (2006) J Mater Chem 16:1273. doi:10.1039/b514565a
10. Hermanek M, Zboril R, Medrik I, Pechousek J, Gregor C (2007) J Am Chem Soc 129:10929. doi:10.1021/ja072918x
11. Zhou W, Tang K, Zeng S, Qi Y (2008) Nanotechnology 19:065602. doi:10.1088/0957-4484/19/6/065602
12. Cornell RM, Schwertfeger U (2003) The Iron Oxides, Viley VCH
13. Hergt R, Hiergeist R, Zeissberger M, Schüler D, Heyen U, Hilger I et al (2005) J Magn Magn Mater 293(205):80–86
14. Welo LA, Baudisch O (1925) Phil Mag 50(IV):399
15. David I, Welch AJE (1956) Trans Faraday Soc 52:1642. doi:10.1039/tf9565201642
16. Massart R (1981) IEEE Trans Magn 17:1247. doi:10.1109/TMAG.1981.1061188
17. Faivre D, Agrinier P, Menguy N, Zuddas P, Pachana K, Gloter A et al (2004) Geochim Cosmochim Acta 68(21):4395. doi:10.1016/j.gca.2004.03.016
18. Vassierres L, Chaneac C, Tronc E, Jolivet JP (1998) J Colloid Interface Sci 205:205. doi:10.1006/jcis.1998.5614
19. Mürbe J, Rechtenbach A, Töpfer J (2008) Mater Chem Phys 110:426. doi:10.1016/j.matchemphys.2008.02.037
20. Dutz S, Hergt R, Mürbe J, Müller R, Zeisberger M, Andrä W et al (2007) J Magn Magn Mater 308:305. doi:10.1016/j.jmmm.2006.06.005
21. Xuan S, Chen M, Hao L, Jiang W, Gong X, Hu Y et al (2008) J Magn Magn Mater 320:164. doi:10.1016/j.jmmm.2007.05.019
22. Gabal MA, Ata-Allah SS (2004) J Phys Chem Solids 65:995. doi:10.1016/j.jpcs.2003.10.059
23. Muan A, Osborn EF (1965) Phase equilibria among oxides in steelmaking. Addison-Wesley Publ. Company, Redding, USA
24. Jørgensen JE, Mosegaard L, Thomsen LE, Jensen TR, Hanson JC (2007) J Solid State Chem 180:180. doi:10.1016/j.jssc.2006.09.033
25. Gillot B (1994) Vibrat Spectr 6:127. doi:10.1016/0924-2031(94)85001-1
26. Kustova GN, Burgina EB, Sadykov VA, Poryvaev SG (1992) Phys Chem Miner 18:379. doi:10.1007/BF00199419
27. Musić S, Popović S, Ristić M (1993) J Mater Sci 28:632. doi:10.1007/BF01151237
28. White WB, DeAngelis BA (1967) Spectrochimica Acta 23A:985
29. Ishii M, Nakahira M, Yamanaka T (1972) Solid State Commun 11:209. doi:10.1016/0038-1098(72)91162-3
30. Coey JMD, Khalafalla D (1972) Phys Status Solidi 11:229. a. doi:10.1002/pssa.2210110125
31. Dunlop DJ (1973). Geophys Res 78(11):1780. doi:10.1029/JB078i011p01780